Lithospheric structure of a nascent spreading ridge inferred from gravity data: The western Gulf of Aden

Hélène Hébert, Christine Deplus, Philippe Huchon, Khaled Khanbari, Laurence Audin

JOURNAL OF GEOPHYSICAL RESEARCH, VOL. 106, NO. B11, PAGES 26,345–26,363 NOVEMBER 10, 2001

Lithospheric structure of a nascent spreading ridge inferred from gravity data: The western Gulf of Aden

Hélène Hébert and Christine Deplus

Laboratoire de Gravimétrie et Géodynamique, Institut de Physique du Globe, Paris, France

Philippe Huchon[1] and Khaled Khanbari[2]

Laboratoire de Géologie, Ecole Normale Supérieure, Paris, France

Laurence Audin

Laboratoire de Tectonique et Mécanique de la Lithosphère, Institut de Physique du Globe, Paris, France

Abstract. The Aden spreading ridge (Somalia/Arabia plate boundary) does not connect directly to the Red Sea spreading ridge. It propagates toward the East African Rift through the Afar depression, where the presence of a hot spot has been postulated from seismological and geochemical evidence. The spreading direction (N37°E) is highly oblique to the overall trend (N90°E) of the ridge. We present and interpret new geophysical data gathered during the Tadjouraden cruise (R/V *L'Atalante*, 1995) in the Gulf of Aden west of 46°E. These data allow us to study the propagation of the ridge toward the Afar and to discuss the processes of the seafloor spreading initiation. We determine the lithospheric structure of the ridge using gravity data gathered during the cruise with the constraint of available refraction data. A striking Bouguer anomaly gradient together with the identification of magnetic anomalies defines the geographical extent of oceanic crust. The inversion of the Bouguer anomaly is performed in terms of variations of crustal thickness only and then discussed with respect to the expected thermal structure of the mantle lithosphere, which should depend not only on the seafloor spreading but also on the hot spot beneath East Africa. Our results allow us to define three distinct lithospheric domains in the western Gulf of Aden. East of 44°45'E the lithosphere displays an oceanic character (thermal subsidence recorded for the last 10 Ma and constant crustal thickness). Between 43°30'E and 44°10'E the lithosphere is of continental type but locally thinned beneath the axial valley. The central domain defined between 44°10'E and 44°45'E is characterized by a transitional lithosphere which can be seen as a stretched continental crust where thick blocks are mixed with thinned crust; it displays en echelon basins that are better interpreted as extension cells rather than accretion cells.

1. Introduction and Objectives

Many detailed geophysical studies over the past 10-15 years have been devoted to refining the understanding of accretionary processes at oceanic spreading ridges. The interpretation of high-resolution multibeam bathymetric data has allowed one to characterize the morphological second-order segmentation of slow spreading ridges, which is associated with a crustal segmentation, as shown from the interpretation of seismic and gravity data [e.g., *Kuo and Forsyth*, 1988; *Tolstoy et al.*, 1993]. Negative residual gravity anomalies located at the centers of segments have been interpreted as reflecting thicker crust, hence a higher magmatic production at the segment centers. This suggests that magma supplies are discontinuous along the axis and that seafloor spreading processes display a three-dimensional pattern. The key parameters controlling the segmentation, the magmatic activity, as well as the morphology, is at first order the spreading rate and at second order the thermal structure of the upper mantle [*Lin and Phipps Morgan*, 1992; *Shaw and Lin*, 1996].

The observed segmentation at slow spreading ridges has been explained as reflecting small-scale upper mantle convection [*Schouten et al.*, 1985] and mechanical responses of the oceanic lithosphere to these processes. However, the origin of the segmentation has been little assessed. The segments are not steady over large periods of time, as shown from off-axis studies located first at some spreading ridge axes and their close off-axis extent (2 to 10 Ma) [*Sloan and Patriat*, 1992; *Rommevaux et al.*, 1994; *Gente et al.*, 1995] and more recently until 29 Ma [*Tucholke et al.*, 1997]. On the other hand, questions regarding the relationship between continental rifting and oceanic spreading ridge segmentation are debated [*Hayward and Ebinger*, 1996]. Is the oceanic

[1]Now at Géosciences Azur, Villefranche-sur-Mer, France.

[2]Now at Faculty of Sciences, Department of Geology, University of Sana'a, Sana'a, Republic of Yemen.

Paper number 2000JB900391.
0148-0227/01/2000JB900391$09.00

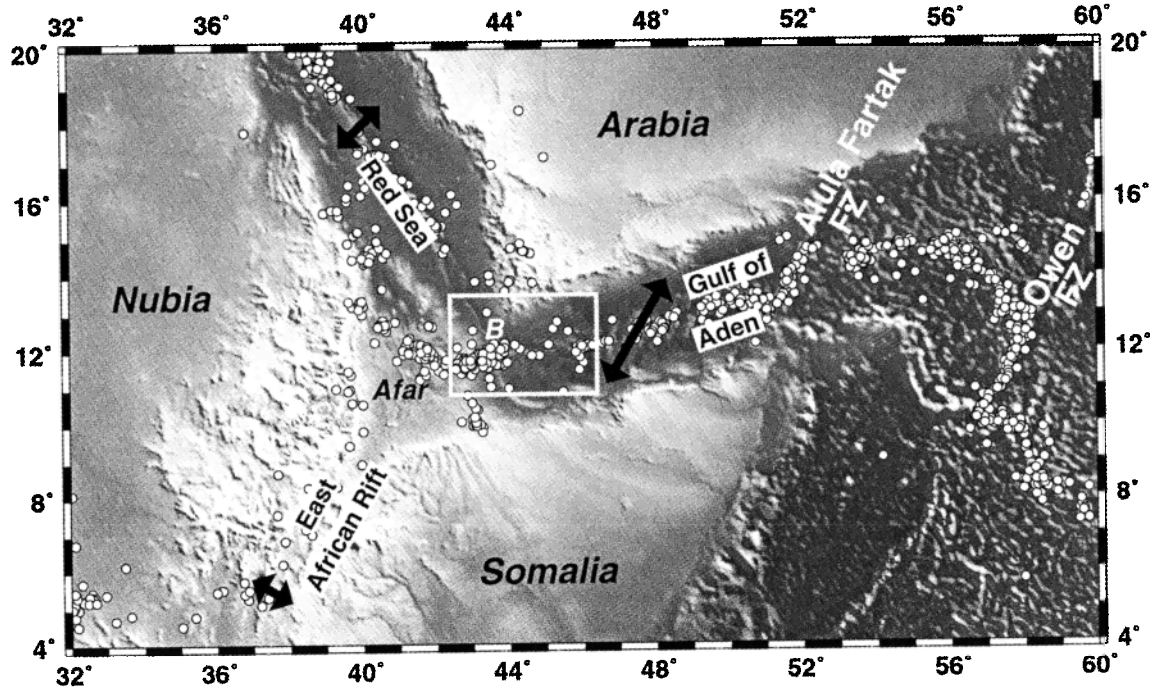

Figure 1. General view of three plate boundaries meeting in East Africa. Bathymetry is that predicted from satellite altimetry [*Smith and Sandwell*, 1997] and topography is from the U.S. Geological Survey (USGS) ETOPO30 DEM. The plate boundaries (among them the Alula Fartak and Owen Fracture Zones (FZ) in the Gulf of Aden) are underlain by global seismicity (USGS data, Preliminary Determination of Epicenters). Solid arrows give the direction and relative rate of opening. In the Gulf of Aden the direction and rate of opening vary from N23°E, 2.4 cm yr^{-1} at 54°E, to N37°E, 1.6 cm yr^{-1} at 44°E [*DeMets et al.*, 1990; *Jestin et al*, 1994]. The Red Sea has opening rates ranging from 0.8 to 1.5 cm yr^{-1} from north to south [*Le Pichon and Gaulier*, 1988], and true oceanic spreading is limited between 18°N and 24°N. The East African Rift is characterized by a very small opening rate (a few mm.yr^{-1}) [e.g., *Jestin et al.*, 1994]. The white rectangle shows the limits of the area surveyed during the Tadjouraden cruise and defines the geographical frame for the next maps. The letter B indicates the Bab el Mandeb strait.

segmentation inherited from rifting characteristics? Is actual oceanic magmatism required for the onset of segmentation? How do the accretion cells initiate and propagate?

We study in this paper the nascent spreading ridge located in the Gulf of Aden west of 46°E, which is propagating toward the Afar depression (East Africa). We aim at characterizing the initiation of the seafloor spreading and the way it propagates into not yet oceanized areas. For that purpose we study the crustal structure of the young spreading ridge through the interpretation of gravity data. First, we define the geographical extent of the actual oceanic crust. Then we discuss the variations of the crustal thickness in order to understand the initiation of seafloor spreading processes. We show that three distinct lithospheric domains can be defined between 43° and 46°E and that only the easternmost domain corresponds to a 10 Ma old well-established seafloor spreading.

2. Geodynamic Setting

The global seismicity data show that three major plate boundaries meet in East Africa. Two submerged boundaries are the oceanic spreading ridges of the Red Sea and of the Gulf of Aden. The third boundary is the continental East African Rift (Figure 1). The two oceanic spreading ridges do not connect to each other through the Bab el Mandeb strait but join the East African Rift in the Afar depression. The Afar area is marked by an intense tectonic and volcanic activity which has been widely studied for years [*Sichler*, 1980; *Courtillot et al.*, 1984; *Tapponnoer et al.*, 1990; *Acton et al.*, 1991; *Gaulier and Huchon*, 1991; *Souriot and Brun*, 1992; *Ebinger and Hayward*, 1996; *Manighetti et al.*, 1998]. The age of beginning of extension in Afar is still controversial but could be as old as 30 Ma. An increase of the magmatic and tectonic activity is proposed to have occurred 10 to 15 Ma ago along the Red Sea and Gulf of Aden, leading to the inception of seafloor spreading in the Red Sea and Gulf of Aden [*Cochran*, 1981; *Izzeldin*, 1987; *Gaulier et al.*, 1988]. In addition, the presence of a hot spot beneath East Africa has been inferred from global tomography [e.g., *Montagner and Tanimoto*, 1990] and geochemical evidence [*Schilling*, 1973; *Vidal et al.*, 1991].

The Aden spreading ridge extends from 58°E in the east, where the Owen Fracture Zone links it to the Carlsberg Ridge in the Indian Ocean, to 43°E in the west, where it propagates toward the Afar depression. Oceanic crust has been identified in the Gulf of Aden from the interpretation of magnetic anomalies which show chron 5 (10 Ma) as the oldest oceanic anomaly along almost the entire Gulf [*Cochran*, 1981]. The magnetic quiet zone beyond chron 5 has been interpreted as contemporaneous with either the stretching of continental crust or early beginning of oceanization, and dated between

10 and 15 Ma [*Cochran*, 1982]. The opening rate decreases from 2.5 cm yr^{-1} at 58°E to 1.5 cm yr^{-1} at 45°E [*DeMets et al.*, 1990; *Jestin et al.*, 1994] while the opening direction varies from N23°E at 54°E to N30°E at 48°E. The opening is thus highly oblique to the mean direction of the ridge (N70°E). Two major fracture zones offset the ridge: the Owen Fracture Zone at 58°E (offset of about 350 km), and the Alulah Fartak Fracture Zone at 52°E (offset of about 180 km) (Figure 1). All these features show that the western Aden spreading ridge might be viewed as a transition zone between the well-established system of Indian Ocean spreading ridges and a continental area of rifting where oceanic accretion does not yet take place.

Recent results concerning the western Aden spreading ridge dealt with models of opening and with the problem of the junction with the Afar depression. As chron 5 is identified along almost the entire Gulf of Aden, the propagation of the opening was probably either instantaneous [*Cochran*, 1981; *Le Pichon and Gaulier*, 1988] or very rapid (at least 10 cm yr^{-1}) with possible slowing down at fracture zones [*Manighetti et al.*, 1997]. Among noteworthy geophysical studies in the western Gulf of Aden, the analysis of gravity and bathymetry profiles with spectral methods has inferred the westward decrease of the equivalent elastic thickness from 15 to 3 km between 52°E and 44°E [*Tamsett*, 1984]. It has been interpreted as resulting from a hotter mantle temperature in the westernmost area, in agreement with the vicinity of a hot spot beneath Afar. A decrease in elastic thickness from 17 to 5 km has also been noticed in the East African Rift, between its southern Ethiopian part and the Afar depression [*Ebinger and Hayward*, 1996]. Simultaneously, the lengths and throws of the border faults decrease as well as the size of the graben; it has been interpreted as an increasing oceanic style in rift segmentation, thus linking the segmentation of a continental rift to the segmentation of oceanic spreading ridges [*Hayward and Ebinger*, 1996]. It is worth noting that a similar decrease in elastic thickness and fault dimensions has been reported along the Reykjanes Ridge, when approaching the influence of the Iceland hot spot [*Searle et al.*, 1998].

The junction with the Afar depression has been debated mainly on the basis of seismological observations, as well as tectonic, magnetic, and topographic data gathered mainly onshore \markcite [e.g., *Courtillot et al.*, 1980; *Lépine and Hirn*, 1992; *Manighetti et al.*, 1998]. Side-scan sonar data had been previously gathered along the axis of the western Gulf of Aden spreading ridge [*Tamsett and Searle*, 1988], as well as limited multibeam bathymetry [*Choukroune et al.*, 1988} and aeromagnetic data [*Courtillot et al.*, 1980}. However, the whole area, as well as the Gulf of Tadjoura and the Ghoubbet, lacked any detailed bathymetric and geophysical data coverage, both on and off axis. The data we interpret in this paper give the opportunity to make a link between pure continental rifting and established oceanic spreading and to propose a model for the initiation of seafloor spreading processes.

3. Data Acquisition

The data we interpret in this paper were gathered during the Tadjouraden cruise (1995) aboard the French R/V *L'Atalante* in the western Gulf of Aden [*Huchon et al.*, 1995]. Multibeam bathymetry and backscatter data were collected with the Simrad EM12D (for areas with depths > 200 m) or EM950 (for shallow areas < 200 m) multibeam echosounders. Such equipment allowed a complete and precise bathymetric coverage (pixel of 50 to 150 m and vertical precision of about 20 m for a 3000 m depth) of the Ghoubbet and the Gulf of Tadjoura, and of the axial area west of 45°40'E (Figure 2) where track spacing was about 1 to 5 nautical miles. Track spacing was increased to about 10 nautical miles in the southern off-axis area. Geophysical data were gathered throughout the survey and consisted of gravity, magnetic, seismic, and 3.5 kHz data. The acquisition of 6-channel seismic data was partial in the Ghoubbet area and in the Bab el Mandeb strait. Moreover seismic acquisition was not performed south of 11°30'N in the Somalian exclusive economic zone (EEZ). Navigation was based on Global Positioning System throughout the survey.

The gravity data were collected using a Bodenseewerk KSS30 gravimeter. According to the two gravity ties performed in Djibouti harbor before and after the cruise, the instrumental drift was close to 0 mGal for the 19 day cruise. The total gravity field was measured every 10 s as well as the heading and speed which allowed us to compute the Eötvös effect. The free air anomaly was obtained by removing the Eötvös effect from the total field and was then sampled to 1 min values using the cubic spline method [*Inoue*, 1986]. The accuracy of free air anomalies is estimated to be 1.5 mGal from the standard deviation of the crossover differences.

4. Characterization of the Spreading Ridge and Identification of the Oceanic Crust

In this section, we first present the main morphological characteristics of the spreading ridge, as well as its free air gravity signature. We then define the geographical extent of the oceanic crust using both the Bouguer anomaly and the magnetic anomalies.

4.1. Morphology of the Spreading Ridge West of 46°E

The multibeam data (Figure 2) show that the axis of the western Aden spreading ridge trends N90°E east of 44°E and becomes N70°E to the west of 44°E, when approaching the Gulf of Tadjoura. It is organized in several oblique N110°E trending basins that are roughly perpendicular to the spreading direction (N37°E). Their maximum depth reaches 1800 m. On a regional scale the axial valley floor deepens toward the Afar depression, up to 43°20'E at the western tip of the westernmost basin. In the Gulf of Tadjoura the individual basins get smaller and shallower. The general off-axis trend is a deepening eastward. The Shukra El Sheik discontinuity, where the existence of a transform fault has been previously proposed [*Cochran*, 1981], is not expressed in the bathymetry.

The sedimentary cover is rather thick in the studied area because the spreading ridge is located close to the continental shelves suppplying a high sedimentation rate in the ocean. The sediment thickness was obtained from recorded seismic data where available and ranges from 0 (in the vicinity of the axial valley) to 2000 m [*Khanbari*, 2000]. When removed from the bathymetric values, they provide the depth of the basement (Figure 3).

Figure 4 shows the free air anomaly map derived from our gravity data. Positive values (10 to 25 mGal) are associated

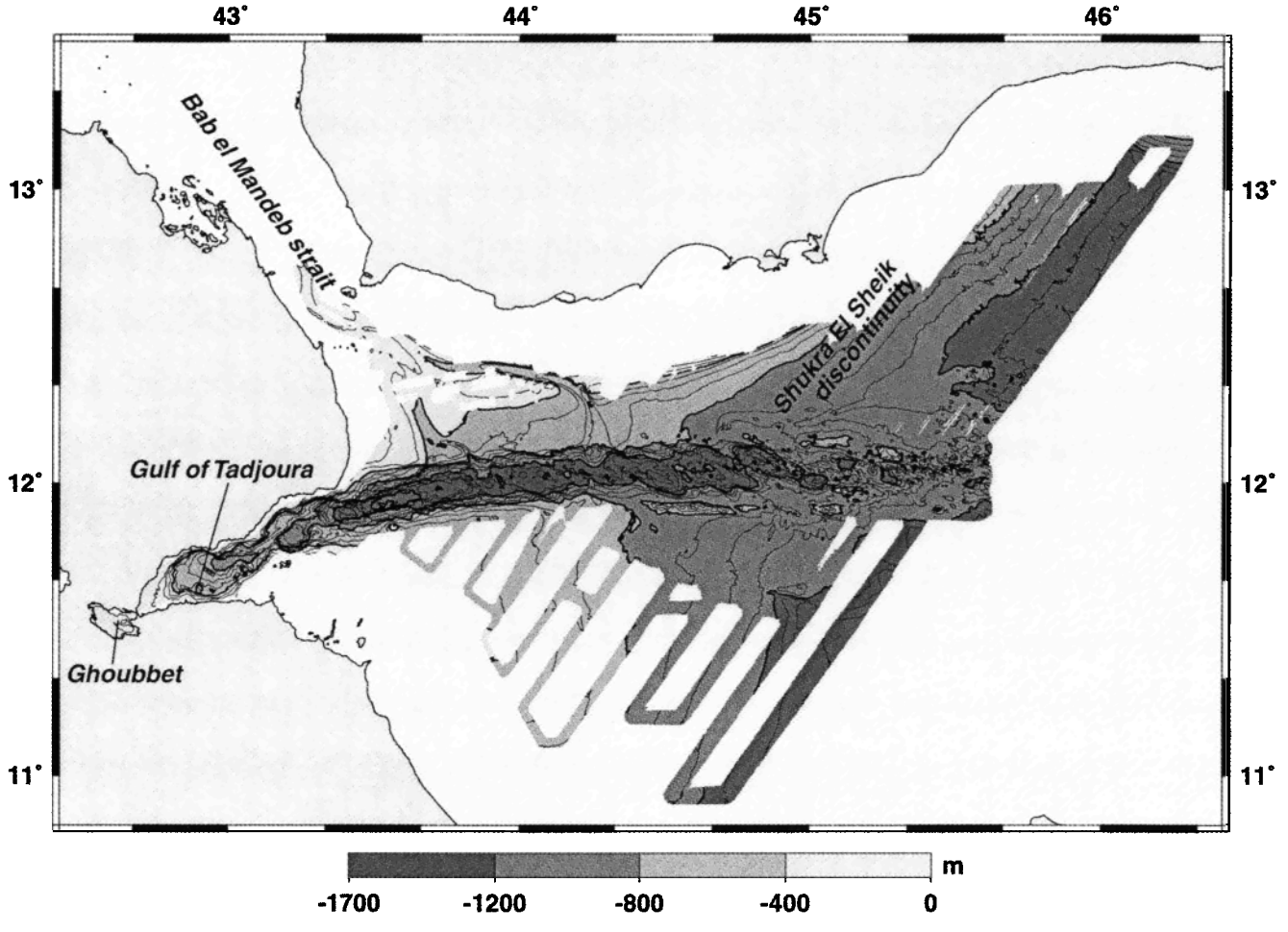

Figure 2. Multibeam bathymetric data gathered during the Tadjouraden cruise aboard R/V *L'Atalante* with Simrad EM12D (depths > 200 m) and EM950 (depths < 200 m) systems. Note the increased spacing between the tracks (about 10 nautical miles) in the southern surveyed area. Contour interval is 100 m, with thicker contours at 400 m intervals. Maximal depth values occur at about 43°30'E, 12°N, in the westernmost axial valley east of the Gulf of Tadjoura, and off axis at the northern and southern extremities of the profiles in the eastern area. Note the presence of two submarine canyons reaching the axial valley near 43°50'E and 44°15'E.

with the quite narrow flank relief and negative values (-25 to -5 mGal) underline the axial valley. A negative anomaly (at least -60 mGal) extends into the Gulf of Tadjoura and Ghoubbet areas westward of the deepest basin. The mixing of our marine gravity data with satellite-derived gravity data has not been performed due to the low accuracy of the satellite-derived gravity data close to the shores: the differences with the marine data show that the satellite-derived data display reduced amplitudes at short wavelengths (20-30 km), as expected, but also that the differences are greater than 65 mGal for larger wavelengths, at distances smaller than 50 km from the coast [*Hébert*, 1998].

The characteristics of the spreading ridge and its evolution from east to west are better illustrated on eight cross sections oriented along the flow lines (Figure 5). The cross sections (located on Figure 4) intersect the center of each basin in order to avoid the presence of two basins along the same profile. The mean axial depth is 1000 to 1500 m, thus at least 1000 m above the value (about 2600 m) predicted from classical subsidence laws [*Parsons and Sclater*, 1977, *Stein and Stein*, 1992]. We can account for this difference by the fact that the spreading ridge has not yet reached a state of equilibrium and is dynamically supported by regional thermal reheating and continental margins. The axial trough deepens westward to achieve depths of at least 1500 m at 43°30'E (profile 8), and this gradual deepening is correlated with an increasingly negative free air anomaly, as already noticed on Figure 4.

4.2. Computation of the Bouguer Anomaly

The oceanic lithosphere is at first order well described by a series of interfaces associated with density contrasts (e.g., water/sediment, sediment/crust, and crust/mantle). Thus the free air anomaly mainly contains the gravity effects of these different interfaces. As we independently know the water/sediment (described by the bathymetry) and the sediment/crust (deduced from seismic data) interfaces, we can subtract their gravity effect from the free air anomaly and thus obtain the "basement Bouguer anomaly" (hereinafter referred to as Bouguer anomaly) which reflects deeper density anomalies.

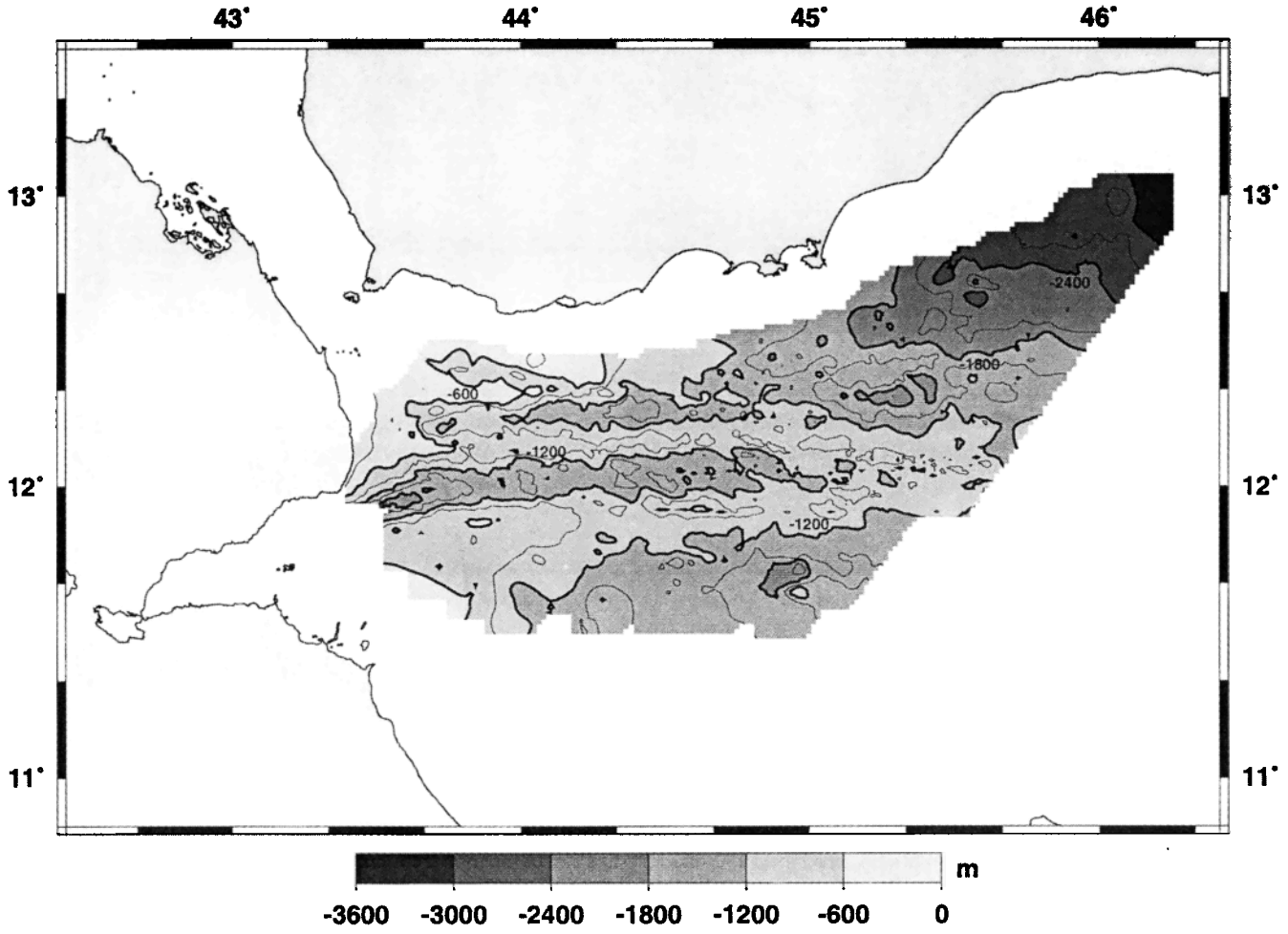

Figure 3. Depth to basement obtained by subtracting from the bathymetry the sediment thickness inferred from seismic data, using the function $T_m = 760\ T_{twt} + 247\ T_{twt}^2 + 17$, with T_m the thickness in meters and T_{twt} the two-way travel time in seconds. Contour interval is 300 m, with thicker contours at 600 m intervals. The acquisition of seismic data was not possible south of 11°30'N. An EW rift parallels the spreading axis can be seen to the north of the axial valley (at about 12°15'N), but there is no southern counterpart. It is not noticeable in the bathymetric map (Figure 2) since it is totally filled with sediments. It may correspond to an aborted rift which was active before it jumped to the south to its present-day location [*Khanbari*, 2000].

So we computed the Bouguer anomaly by subtracting three distinct terms from the free air anomaly. We first took into account the gravity effect of the bathymetry considered as a water-sediment interface. Second, we computed the effect of the surrounding topographic relief which exhibit heights rapidly increasing away from the coast (north of the Gulf of Tadjoura, the altitude reaches 1600 m above sea level about 10 km inland). The third contribution is the topography of the top of the oceanic crust deduced from seismic data.

An efficient fast Fourier transform method [*Parker*, 1972] is often used in marine surveys to compute the Bouguer anomaly in the spectral domain, but it could not be easily applied in our case for the two following reasons. First, the study area includes coastal zones where shallow depths would require a very small grid spacing, hence increase computation times and possibly lead to numerical instabilities. Second, the surveyed area is surrounded by emerged relief that could not be easily taken into account using this method. So we used an analytical three-dimensional (3-D) xcalculation based on the algorithm of *Chapman* [1979]. The gravity effect of each density interface is computed as a series of triangular facets defined by points on the rectangular grid at the depth of the interface. The method is fully described by *Rommevaux et al.* [1994]. It allows us to compute the gravity effect directly at measurement points and to take into account both bathymetry and topography [*Deplus et al.*, 1996].

In order to compute the gravity effect of the bathymetry and topography interfaces, a digital elevation model has been first constructed over a large zone (500 by 450 km) encompassing our studied area. In the marine area, where our gravity data are located, we used multibeam bathymetric data gathered during the cruise. Their high resolution could provide 100 m spacing grids. Several tests have been performed in order to determine the optimum spacing for computation of gravity effects at sea level. Using a 1 km grid spacing rather than a 100 m spacing yields differences smaller than 0.5 mGal in areas of steep slopes [*Hébert*, 1998], thus smaller than the precision of the marine gravity data. We chose a 1 km spacing for our final digital elevation model (DEM). To extend the coverage we added ETOPO5

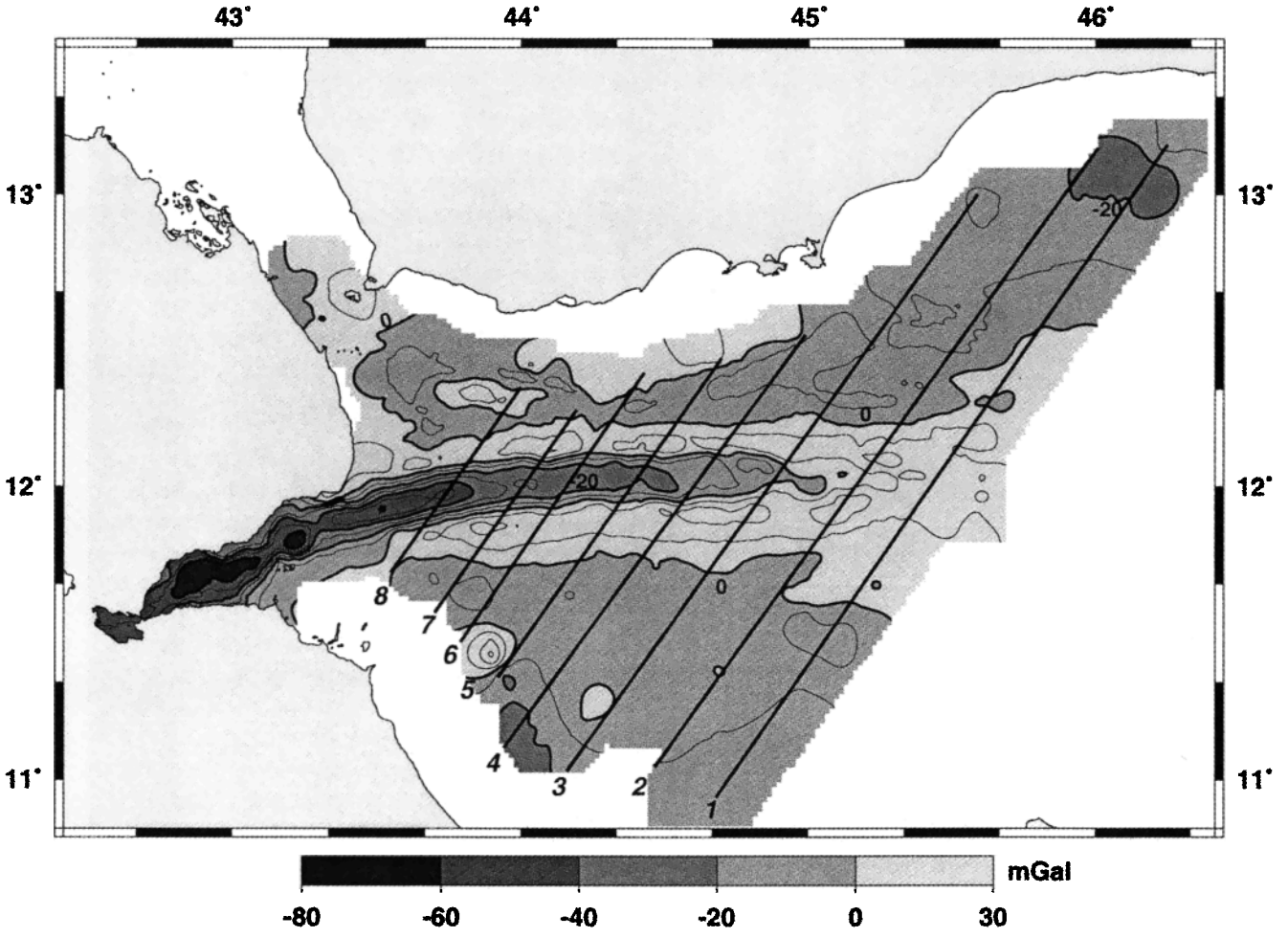

Figure 4. Free air anomaly computed from the Bodenseewerk gravity data merged with the GPS navigation. For drawing purposes the gravity values gathered along tracks have been sampled on a 1 km grid using the adjustable tension surface gridding algorithm from the Generic Mapping Tools (GMT) software. Contours at 10 mGal intervals are shown, with thicker contours at 20 mGal intervals. Numbered lines indicate the locations of the profiles displayed in Figure 5.

bathymetric data for marine areas and ETOPO30 topographic data for land. ETOPO5 data (grid spacing 5') are a compilation and interpolation of data from existing cruises, and in the western Gulf of Aden their long-wavelength trend is close to our averaged multibeam bathymetric data [*Hébert*, 1998]. The ETOPO30 data consist of a DEM at 30" spacing for East Africa. We first projected the ETOPO5 and ETOPO30 data in the same Mercator system as our multibeam data. Then the available data were merged with the multibeam grid to define nodes of a 1 km spacing grid, and the gaps were interpolated using the Generic Mapping Tools (GMT) gridding algorithm with a tension factor of 0.1. Our final DEM is a 1 km spacing grid, extending at least to 50 km from the measurements points in order to reduce any step-like edge effect.

Seismic data were not recorded in the southern part of the survey (south of 11°30'N) where sediment thickness cannot be neglected. In order to avoid long-wavelength artifacts in the Bouguer anomaly, we introduced reasonable mean values of sediment thickness in this area. We computed the sediment thickness where seismic data were not gathered (south of 11°30'N) as an analytical function of the bathymetric values along each NE-SW profiles (Figure 6). The observed and predicted basement depths were then gridded on a regular 1 km grid with fixed zero values for emerged areas.

We chose the same density (2700 kg m^{-3}) for oceanic and continental crust; the gravity influence of the latter is maximum in the first kilometers offshore (4 to 5 mGal). The density chosen for the sediments (2200 kg m^{-3}) is an average value that does not take into account heterogeneities within the sedimentary layer. However, it allows us to compute a reasonable gravity effect in regions covered with sediments, particularly near the coast. In addition, the gravity effect of coastal relief is maximum in the same areas, and since the procedure used to define basement in areas devoid of seismic data is not exact either, the Bouguer anomaly will display a lower precision near the coast, at the ends of the profiles. Thus we must keep in mind that these areas have to be interpreted with caution.

The bathymetry, topography, and basement grids were used to compute the gravity effects at each data point. The reference depth was chosen as 0 km so that all computations are homogeneous and the obtained Bouguer anomaly can be directly mixed with the inland Bouguer anomaly for future

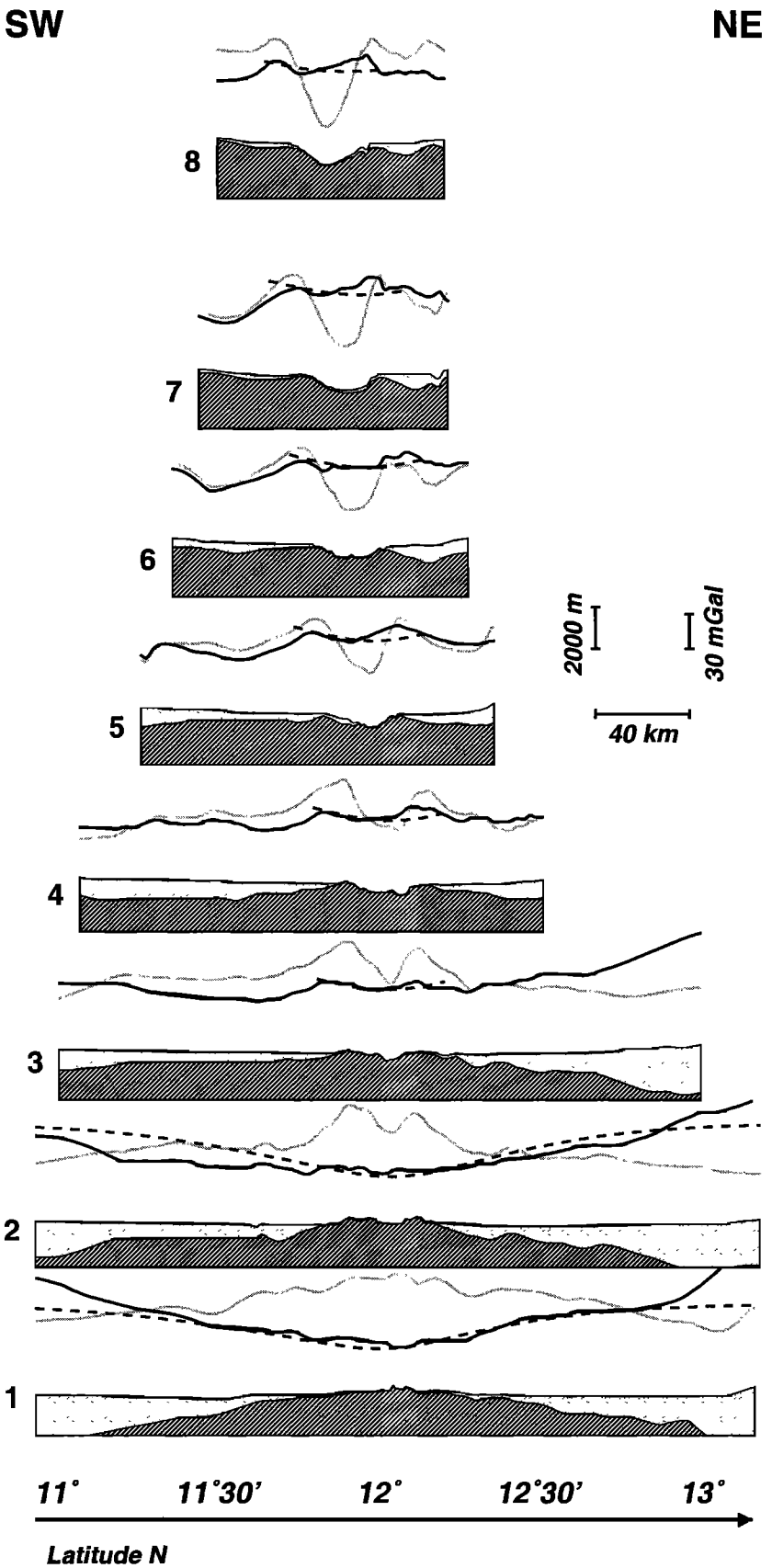

Figure 5. Cross sections of the western Gulf of Aden spreading ridge (located on Figure 4). Each profile is oriented along the opening direction (N37°E), thus perpendicular to the basins plotted in Plate 1 (except for basin 8 which trends N70°E). The oceanic crust is shown in dark grey, and light grey is for the sediment cover deduced from seismic data. Minimal depth value is -3500 m for each profile. Grey solid line is the free air anomaly. Black solid line represents the mantle Bouguer anomaly as shown in Plate 2 (i.e., Bouguer anomaly minus gravity effect of the a priori model for the Moho geometry). The thermal effect (black dashed lines) has been computed with a half-space cooling plate model, as explained in section 6. All bathymetry and gravity values are extracted from gridded data.

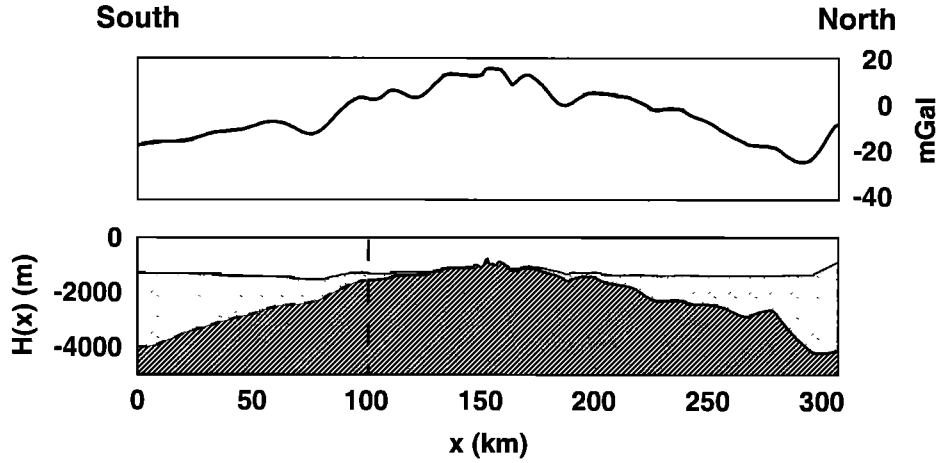

Figure 6. Sketch of the method used to derive basement in areas without seismic data, south of 11°30'N. This profile is a cross section perpendicular to the axial valley. In the southern part ($x < 100$ km) the sediment thickness $T(x)$ has been obtained as an analytical transform of the bathymetry $H(x)$, with $T(x) = T_0 + t.H(x).(x-x_0)^2$, with t and T_0 being adjusted for each profile from comparison between the assumed basement and the short wavelength of free air anomaly, where bathymetry is flat (top profile).

work. The sum of the three effects was subtracted from the free air value at each data point to obtain the Bouguer anomaly.

4.3. The Bouguer Anomaly

The Bouguer anomaly (Plate 1) provides indications of the crustal and lithospheric structure beneath the area since we removed the predictable effects of surficial density contrasts: at first order, it reflects crustal thickness variations as well as thermal anomalies in the upper mantle. A negative (positive) Bouguer anomaly can reflect thick (thin) crust or the presence of low density/hot temperature related to an asthenospheric upwelling (high density/cold temperature).

A large regional EW trend dominates the Bouguer anomaly and ranges from -50 mGal in the west to 90-130 mGal in the east, depending on axial or off-axis values. This trend is probably mainly related to the continent-ocean transition. Though our study area does not extend farther into Afar, we can not rule out a thermal origin for this regional trend: hotter and shallower mantle beneath East Africa could be responsible for the regional negative density anomaly. However, the exact mantle temperature distribution in such a context is unclear since the propagating spreading ridge is certainly associated with a hot and shallow mantle temperature as well. In addition the thermal density contrast is probably small (about –60 kg m^{-3}). Therefore it is reasonable to assume that the long-wavelength Bouguer anomaly is mainly controlled by the continent/ocean crustal transition since the Moho is associated with a higher density contrast (2700/3300 kg m^{-3}) and the crustal thickness variation is large.

Apart from the large westward decrease, the main feature of the Bouguer anomaly is a striking linear gradient which defines a triangular area. The triangle points toward the Afar, ends at 43°30'E, and widens to the east. The Bouguer anomaly is more positive within the triangle and reflects a thinner crust, compatible with the presence of oceanic crust. Plate 1 also displays the magnetic anomalies identified from the magnetic data gathered during the cruise [*Audin*, 1999], using the *Sloan and Patriat* [1992] timescale. Thus the Bouguer anomaly together with the magnetic anomalies allows us to define at first order the geographical extent of oceanic crust in the western Gulf of Aden. This area ends to the west near 44°E, where the seafloor spreading has not yet reached the westernmost region. This result is compatible with the presence of thick, possibly stretched crust in the Gulf of Tadjoura. In addition, we note that the Bab el Mandeb strait is not associated with a positive Bouguer anomaly, and this confirms that the area is unlikely to be characterized by seafloor spreading.

5. Inversion of the Bouguer Anomaly

5.1. Method

We aim at determining the geometry of the crust/mantle interface from the inversion of the Bouguer anomaly. However, the Bouguer anomaly also contains the gravity effect of thermal anomalies. As mentioned before, the actual depth of the isotherms in the studied context is difficult to establish. Thus we first invert the Bouguer anomaly attributing all sources as Moho topography. Then the computed crustal thickness is discussed in light of possible additional thermal anomalies related to the hot spot and the spreading ridge.

In most recent studies of oceanic spreading ridges, residual mantle Bouguer anomalies are usually computed by subtracting from the Bouguer anomaly the gravity effect of a 6 km constant thickness crust and the effect of density variations due to the cooling of the lithosphere [e.g., *Phipps Morgan and Forsyth*, 1988]. Then the residual anomalies are assumed to be only due to crustal thickness variations with respect to the constant thickness crust model. However, such a method cannot be applied in the western Gulf of Aden where the Bouguer anomaly is dominated by the decrease of crustal thickness across the continent/ocean boundary. This decrease produces a west-east long-wavelength anomaly and defines a high gradient line bounding the oceanic crust area. In this case we chose to construct a different a priori model based on other available data.

The way we invert the Bouguer anomaly is thus to (1)

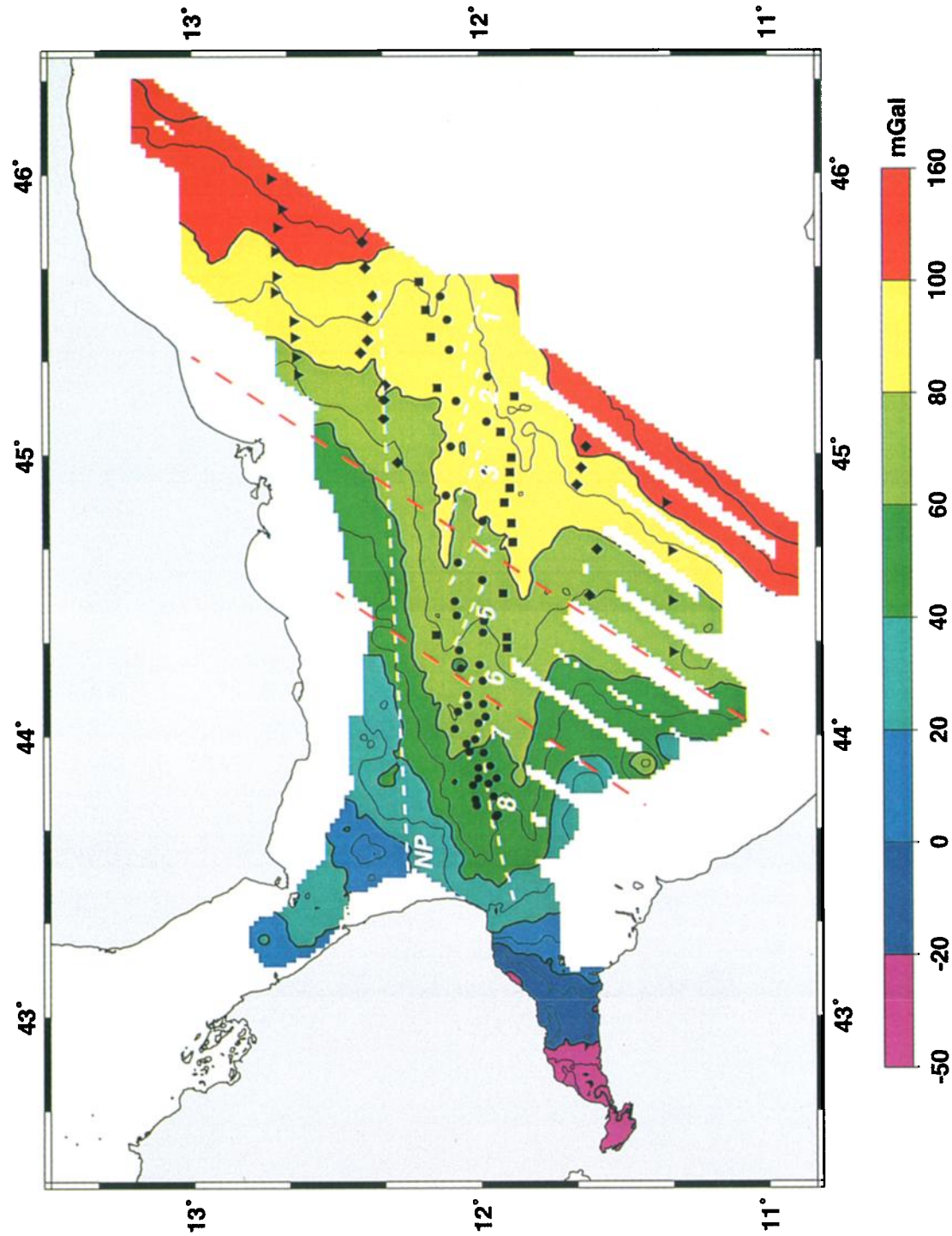

Plate 1. Basement Bouguer anomaly computed by removing from the free air anomaly the attractions of water-sediment (1030/2200 kg m^{-3}), sediment-crust (2000/2700 kg m^{-3}), and air-crust (0/2700 kg m^{-3}) (inland) interfaces (see text for details). Solid symbols correspond to magnetic anomalies: upper boundary of chron 5 (10.1 Ma) (inverse triangles), chron 3 (3.9 Ma) (diamonds), chron 2 (1.9 Ma) (squares), and Brunhes-Matuyama transition (0.8 Ma) (circles). In the axial valley, each basin (white dashed line) is defined by the locally maximum depth and is identified by white numbers. The sections across and along the basins are plotted on Figures 5 and 8, respectively. The northern profile (NP) is plotted on Figure 8. The red dashed lines define the three lithospheric domains discussed in sections 6 and 7.

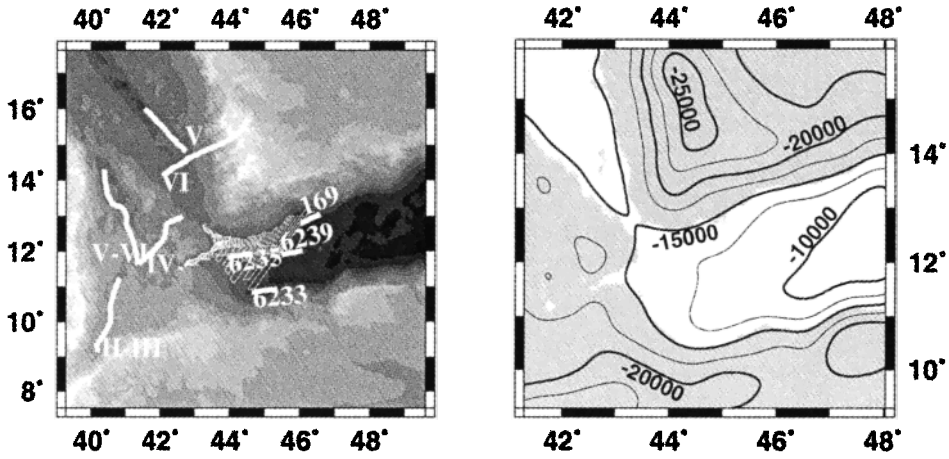

Afar refraction lines

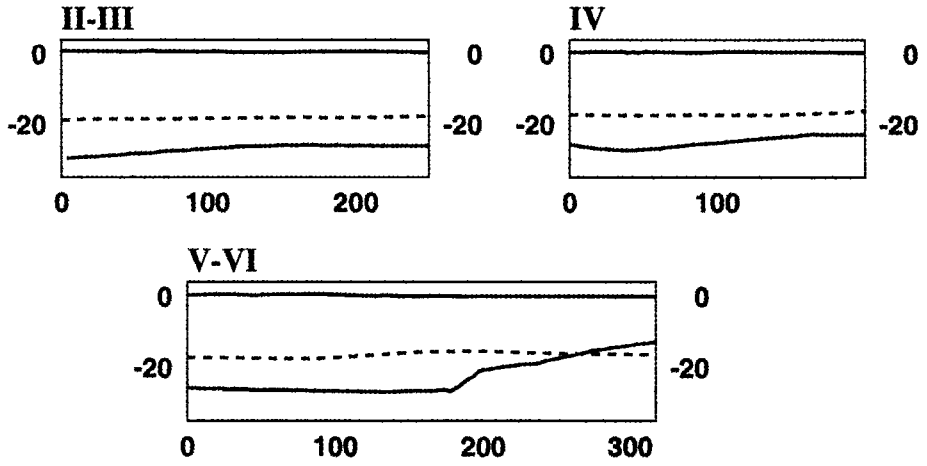

Red Sea refraction lines

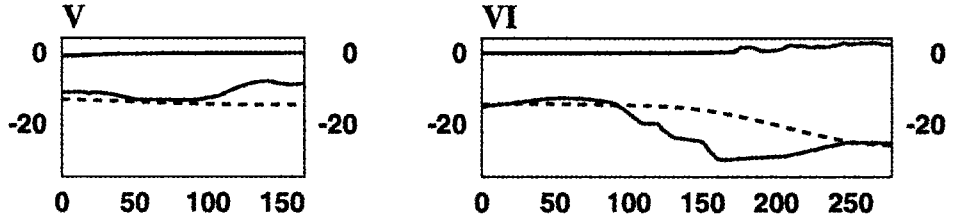

Gulf of Aden data

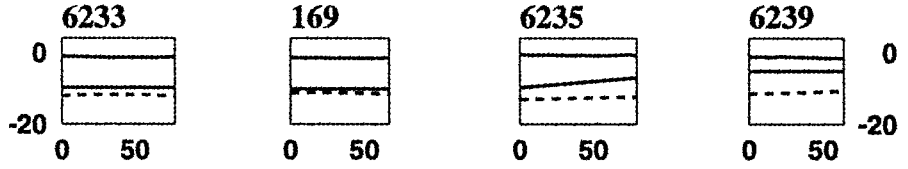

Figure 7. Location of the available refraction lines in the area (top left). The Gulf of Aden profiles are from *Laughton and Tramontini* [1969], the Red Sea profiles from *Egloff et al.* [1991], and the Afar data come from *Makris and Ginzburg* [1987]. The a priori Moho (top right) was constructed from an elastic model of the lithosphere (with T_e = 5 km) submitted to topographic loads. We used the Red Sea V-VI lines to constrain the depth of the edges of the a priori Moho model (see text). Profiles show the comparison between the refraction data (continuous line) and our a priori Moho (dashed line). All values are in kilometers.

assume the Bouguer anomaly is due to crustal thickness variations only, (2) subtract from the Bouguer anomaly the gravity effect of an a priori model for the Moho interface, to account for the west-east long-wavelength trend due to the decrease of crustal thickness, (3) compute the second-order crustal thickness variations with respect to this a priori Moho model (these crustal thickness values still contain information on thermal anomalies, and we call them pseudocrustal thickness), and (4) discuss the obtained values taking into account the possible effect of thermal anomalies.

5.2. A Priori Model for the Moho Geometry

To construct our a priori model for the regional Moho interface, we assume that the continental margin is in regional equilibrium on an equivalent elastic lithosphere, with a low rigidity given by an elastic thickness (T_e) of 5 km. Such models have already been suggested to account for continental margin transitions at this wavelength [e.g., *Diament et al.*, 1985]. It has been proposed that the lithosphere has significant strength during rifting and stretching but that it may approach a state of local isostasy at breakup [*Keen and Dehler*, 1997]. In addition, the chosen elastic thickness is in agreement with values obtained in the area (see section 2). The Moho geometry was thus computed from the topography and the bathymetry assuming a $T_e = 5$ km and using different density contrasts depending on aerial topography (0/2700 kg m^{-3}) or seafloor bathymetry (1030/2700 kg m^{-3}). The grid we used to perform the computation was constructed in the same way as the one for the Bouguer anomaly but with a larger size. However, this computation provides the variations of the Moho depth (the grid edges have fixed zero values), but no absolute value. We need independent data to adjust our reference level: the seismic refraction data available in the area provide indications for the thickness of the crust.

Figure 7 shows a compilation of refraction data available in the region. Long profiles in the Afar depression have shown the gradual thinning of the crust toward the Red Sea and the Gulf of Aden [*Makris and Ginzburg*, 1987]. However, this depression is affected by an intense extensional deformation; thus the area has not reached a state of equilibrium and the profiles cannot be used as references. The short profiles in the western Gulf of Aden are quite sparse and do not extend into the continental domain [*Laughton and Tramontini*, 1969]. Thus we chose the Red Sea-Yemen profiles [*Egloff et al.*, 1991] to constrain the reference level of our model of Moho. Indeed, the profile VI on the Yemen margin represents a typical section of a continental margin reflecting the crustal thinning from 25 to 15 km (Figure 7). In addition the south Yemen margin may be less influenced by the conjugate vicinity of the hot spot and the spreading ridges, since the Red Sea is not yet oceanic south of 14°-16°N [*Egloff et al.*, 1991] and should be close to a state of equilibrium. We thus used the Red Sea lines V-VI to constrain the depth of the edges of our a priori Moho model and we obtain 18 km for this reference depth. The Moho geometry computed is contoured in Figure 7, and values extracted from the grid are compared with other refraction profiles.

We note the good agreement for the long-wavelength trend for both southern Red Sea profiles as expected but also for the Gulf of Aden margins (lines 169 and 6233). Figure 7 also shows that such a reference depth does not allow us to fit all the refraction lines. In the Afar depression our flexure model is indeed systematically shallower than the seismic Moho, which was in addition probably identified as too shallow in the 1970s works. The Afar area undergoes intense extensional deformation and thus a model of an elastic plate is not realistic in this case. Lithospheric thinning and concentration of stresses may indeed exist at the edges of the depression where the deformation is more localized [*Manighetti et al.*, 1998]. It may induce a mechanical decoupling there, yielding a collapse of the crust with respect to the equilibrium model, as in models proposed for the formation of the axial valley at slow spreading ridges [*Neumann and Forsyth*, 1993]: mechanically the Afar depression looks like a huge axial valley of an oceanic spreading ridge. In the western Aden spreading ridge the mean depths of Moho predicted from our model display deeper values for axial profiles 6235 and 6239. We already mentioned that the mean axial depth is shallow with respect to the mean depth of world spreading ridges. This is in favor of a dynamic support of the lithosphere at the axis leading to Moho depths shallower than predicted from the regional isostatic model.

Our a priori model for the Moho geometry is thus too deep beneath the spreading ridge and too shallow beneath the Afar. We thus expect that its gravity effect will not completely explain the amplitude of the long-wavelength observed in the Bouguer anomaly but that it will provide a mantle Bouguer anomaly we can then interpret in terms of deviations with respect to the a priori model.

5.3. Mantle Bouguer Anomaly and Pseudocrustal Thickness Variations

The gravity effect of the a priori Moho was computed using four terms in the *Parker* [1972] series, assuming a density contrast of 2700/3300 kg m^{-3} and a reference depth of 18 km, as established before. Figure 8 shows an along-axis gravity profile (axial) and an off-axis one (NP) (see location on Plate 1). Both Bouguer anomaly long-wavelengths are well fitted by the gravity effect of our a priori Moho. In detail, the off-axis (NP) profiles (grey lines) display expected deviations since the model of Moho (dashed) is too shallow in the western area. The axial profiles (black lines) show that the eastern Bouguer anomaly (solid line) is not entirely explained with the model (dashed line), suggesting that an additional density decrease must occur below the axis, in agreement with a hotter temperature in the mantle associated with the spreading ridge.

The gravity effect of the a priori Moho model was subtracted from the Bouguer anomaly to yield the mantle Bouguer anomaly (MBA) (Plate 2); it must be stressed that our MBA differs from the one usually computed at spreading ridges since we use an a priori crust with a variable thickness and not a constant one. This map allows us to define three domains as a function of their across-axis MBA variations and separated by red lines on Plate 2. East of 44°45'E (domain I), the MBA strongly increases from the axis to both flanks by about 70 mGal. From 44°10'E to 44°45'E (domain II), the MBA is quite constant and displays two relative maxima (10-20 mGal) associated with the flanks of the axial domain. West of 44°10'E (domain III), the MBA still displays the two relative maxima but decreases from the axis to the flanks (about 25-30 mGal).

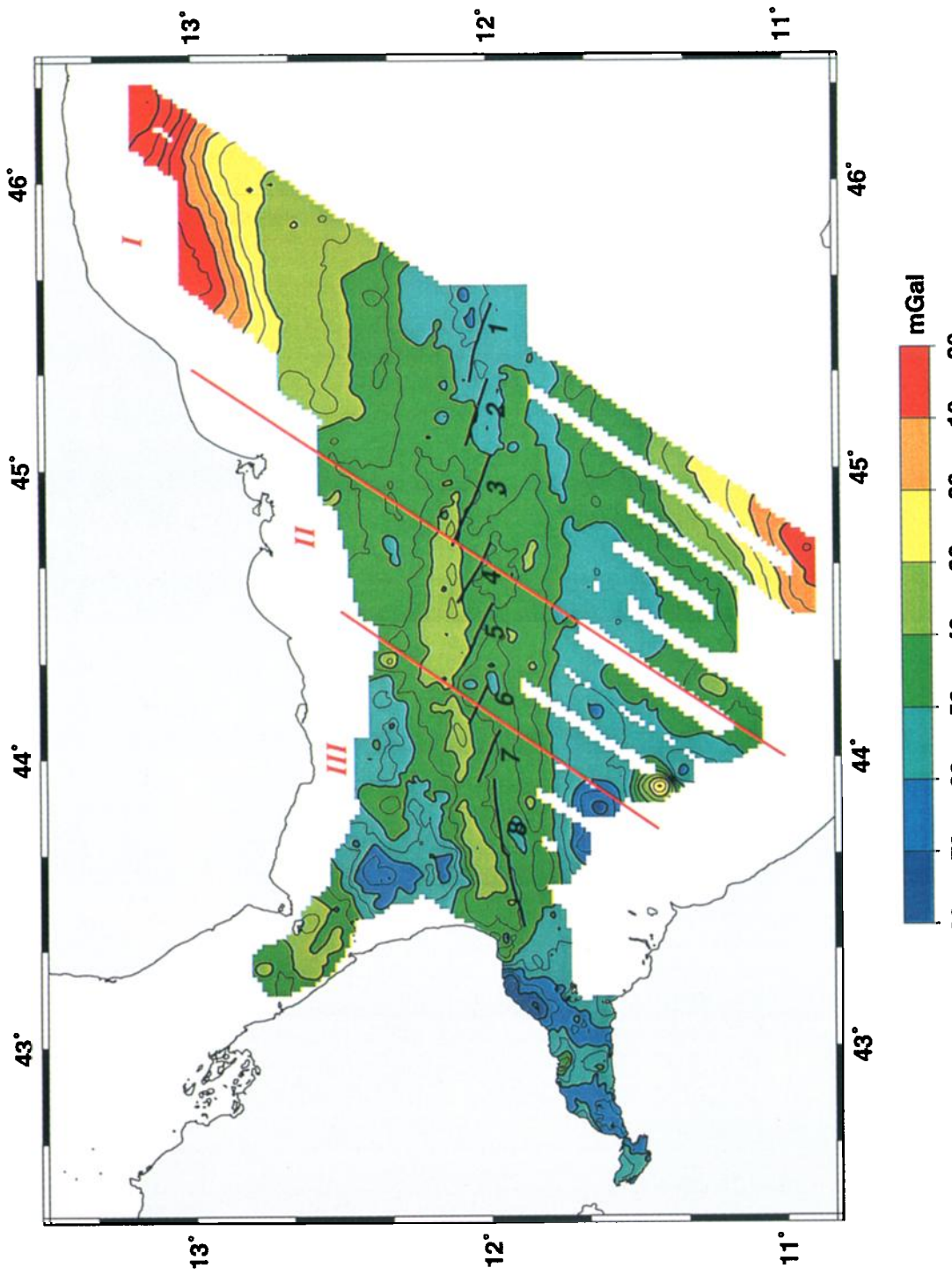

Plate 2. Mantle Bouguer anomaly obtained by subtracting from the Bouguer anomaly the gravity effect of the model of Moho (density contrast 2700/3300 kg m^{-3}). The long-wavelength Bouguer anomaly related to the continent-ocean crustal transition has been reduced along the axis. A relatively low anomaly underlines the axial valley with respect to the flanks. A very negative anomaly is still present close to the Gulf of Tadjoura and the Bab el Mandeb strait. The red lines define the three lithospheric domains I, II, and III discussed in the text.

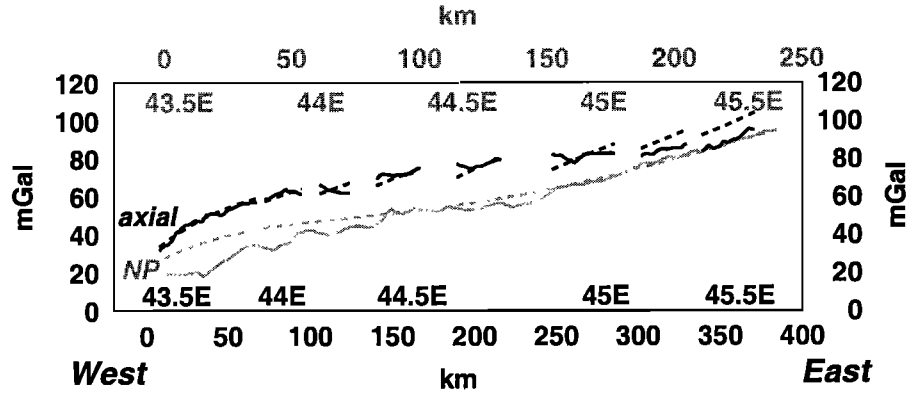

Figure 8. Cross sections along the axial basins (black) and along the NP off axis profile (grey) (location on Plate 1). Bouguer anomaly (solid line) and effect of the a priori Moho (dashed line). The longitude references are not linear for axial profiles since basins do not trend N90°E. The long-wavelength Bouguer anomaly is well explained by the a priori Moho model, and the observed deviations are discussed in the text.

The mantle Bouguer anomaly still contains the effect of density variations associated with thermal anomalies. For example, in domain I the long-wavelength along flow lines is similar to the one observed at slow spreading ridges [e.g., *Rommevaux et al.*, 1994]. This long-wavelength anomaly consists of a relative negative anomaly beneath the axis and is explained by the hotter mantle associated with the asthenospheric upwelling. Such a trend along flow lines is also clearly shown in our profiles (Figure 5, black lines), and its amplitude reaches more than 70 mGal (profiles 1 and 2). The mantle Bouguer anomaly may be overestimated at the end of the profiles since the density and/or thickness of the sediments may be underestimated. Profiles 4 to 6 (domain II) do not display such a long-wavelength trend and well illustrate the two relative anomaly highs (10-20 mGal) associated with the flanks of the axial domain. Profile 3 appears as a transition profile where a long-wavelength still exists and coexists with two low flank highs (5-10 mGal). In domain II the axis is also underlain by a negative anomaly but of much smaller amplitude than in domain I. This anomaly is probably partly due to a thermal origin.

Upwelling of the asthenosphere beneath the Aden ridge axis may contribute to the mantle Bouguer anomaly at both small and large wavelength. Therefore it is difficult to remove its effect by forward modeling or by filtering the anomaly. This explains why we prefer to invert the MBA in term of crustal thickness variations only and then to discuss the results in term of possible additional thermal anomalies.

The inversion of the mantle Bouguer anomaly was performed using a Fourier domain method [*Oldenburg*, 1974]. This iterative method is based on the direct spectral formula [*Parker*, 1972] used to deduce the interface h responsible for the observed anomaly g. Assuming k is the wavenumber, z is the reference depth, FT is the Fourier Transform, and $\Delta\rho$ is the density contrast:

$$FT[h] = \frac{e^{kz}}{2\pi G\Delta\rho} FT[g] - \sum_{n=2}^{\infty} \frac{|k|^{n-1}}{n!} FT[h^n].$$

This method strongly depends on the low-pass filter applied to limit numerical instabilities in the exponential term and on the chosen reference depth. The computation was performed on a square grid for which the reference depth can be derived from the model of the Moho, and is chosen at 12 km. The cutoff wavelength can be roughly estimated by assuming spherical point sources buried at depth h which produce anomalies with wavelength $1.5h$. In our case all wavelengths lower than 22 km were cut off with the filter proposed by *Oldenburg* [1974]. The density contrast is 2700/3300 kg m^{-3}, and four iterations were necessary to finally obtain a 2 mGal RMS. The results of the inversion are added to the a priori Moho to obtain the crust-mantle interface deduced from gravity data. When subtracted from the estimated depths to basement, this yields the pseudocrustal thickness map (Figure 9).

6. Results: Crustal Structure of the Spreading Ridge

The values obtained for pseudocrustal thickness range from 5 to about 21 km, with maxima reached in localized areas such as in the Bab el Mandeb straits and in the Gulf of Tadjoura. They may indicate the presence of isolated continental crustal bodies corresponding to tilted blocks inherited from the rifting. Mean values east of 44°10'E range from 8 to 12 km and confirm the extent of the oceanized area defined in the previous section from the Bouguer anomaly.

As previously mentioned, the pseudocrustal thickness still contains the gravity effect of thermal anomalies. For example, the entire axial valley is underlain by a relative apparent crustal thickening with respect to the flanks (west of 44°45'E) and to the off-axis domain (east of 44°45'E). The probable presence of hot mantle beneath the axial area is, however, in favor of a thermal origin for this apparent crustal thickening.

In order to discuss the possible influence of the asthenospheric upwelling associated with the spreading ridge, we estimated the geometry of the lithosphere/asthenosphere boundary resulting from its deepening with age. This geometry is provided by the half-space cooling plate model [*Parsons and Sclater*, 1977] with the ages given by the magnetic anomalies. Then the gravity effect of this lithosphere/asthenosphere interface was computed with the Parker algorithm and a density contrast of -60 kg m^{-3} (Figure 10 (top) and dashed lines on Figure 5). Such a method

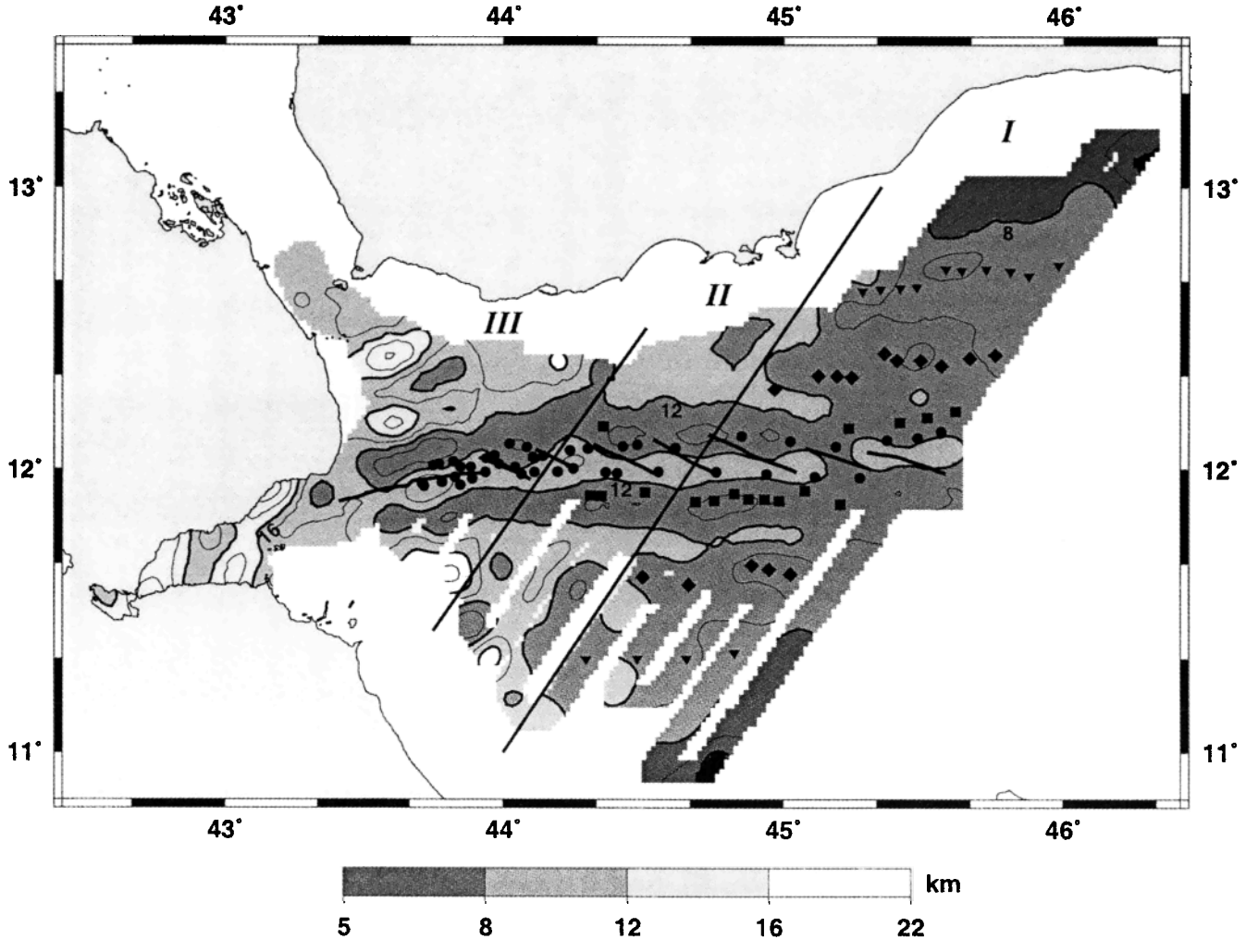

Figure 9. Pseudocrustal thickness obtained from the inversion of the mantle Bouguer anomaly. Contour interval is 2 km, with thicker contours at 4 km intervals. Gravity effects of thermal anomalies are still contained in the resulting crustal thickness. Therefore the thickening observed at the axis east of 45°E could be explained by asthenospheric upwelling. Black solid lines and symbols: axial basins and magnetic anomalies as on Plate 1.

has been compared by *Rommevaux et al.* [1994] with the one [*Kuo and Forsyth*, 1988] using a 3-D mantle temperature distribution. The difference between gravity effects is smaller than ± 2 mGal in case of small offsets of the ridge axis, as in our study area. In addition, it allows to take into account asymmetry and spreading rate variations since we use observed magnetic anomalies. As the oceanic crust does not extend in the whole area, this computation is only approximate and is not valid where magnetic anomalies are not recognized. Therefore we avoided to subtract the resulting gravity effect and instead we preferred to compute the equivalent crustal thickness variations inferred from the gravity effect of the lithosphere/asthenosphere interface (Figure 10 bottom) with the same method and parameters as for the inversion of the mantle Bouguer anomaly.

In domain I the 4 km thickening computed with this method beneath the axial area with respect to the off-axis domain seems to explain the pseudo thickening observed east of 45°E in Figure 9. Figure 5 confirms that the long-wavelength of the mantle Bouguer anomaly along flow lines is satisfactorily fitted by the gravity effect of the lithosphere/asthenosphere boundary (dashed line) for profiles 1 and 2. The mantle Bouguer anomaly at the end of these profiles may be overestimated due to a poor correction for the sedimentary layer, or the crust is really thicker due to the beginning of the continental margin. Therefore if we exclude the ends of the profiles, then this implies that the thickness of the oceanic crust is rather constant along these profiles and amounts to about 8 km.

In domain II, though the magnetic anomalies are identified to chron 2 (1.86 Ma) only in the area west of 44°45'E, the gravity effect due to the asthenospheric upwelling fits rather well the 50 km wide axial zone, as shown in profiles 4 to 6 (Figure 5). The northern flank remains underlain by a positive anomaly with respect to the thermal gravity effect. Nevertheless, the relatively large pseudocrustal thickness observed at the axis between 44°10'E and 44°45'E is reasonably well explained by the thermal effect. Thus we can infer that the mean thickness of the crust in the axial area is about 10-12 km, in good agreement with the refraction line 6235 (Figure 7) that was not used to constrain the a priori model.

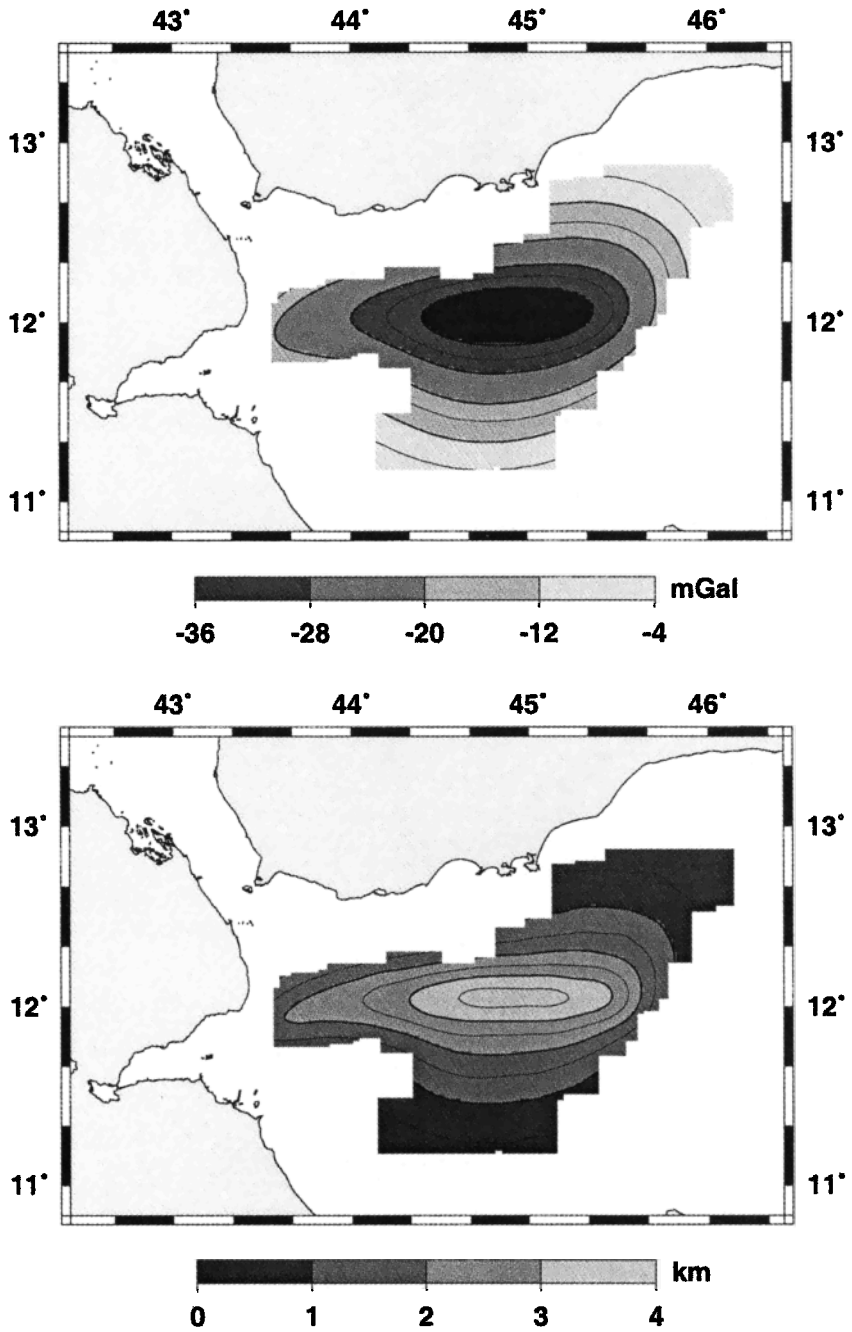

Figure 10. Gravity effect computed from a simple cooling model of the lithosphere/asthenosphere boundary. This effect was then converted to crustal thickness variations by applying the same method of inversion as for the mantle Bouguer anomaly and the same parameters. This computation was done for comparison with the pseudocrustal thickness variations in domains I and II.

As for domain III (profiles 7 and 8 in Figure 5) the thermal effect does not explain the mantle Bouguer anomaly, and the higher anomaly associated with the northern flank seems to extend to the axial zone. A southward offset between the deep crustal structure and the surface features is noticed and more pronounced than in domain II, so the crustal layer is clearly asymmetric.

7. Discussion and Conclusions

These results suggest that three distinct lithospheric domains can be identified in the Gulf of Aden west of 46°E (Figure 11). In the easternmost area (domain I), true oceanic accretion has existed for at least 10 Ma (chron 5) and the crust is essentially oceanic from north to south, with a well-pronounced subsidence from axis, and a rather constant thickness (about 8 km). The classical thermal model for cooling of the oceanic lithosphere as a function of the age well explains the corresponding long-wavelength of the Bouguer anomaly (profiles 1 and 2, Figure 5). In addition, axial volcanic activity seems to be important and recent there: backscatter data show that most of the valley floor is covered with fresh lava flows [*Dauteuil et al.*, 2001].

In the middle part of the surveyed area (domain II),

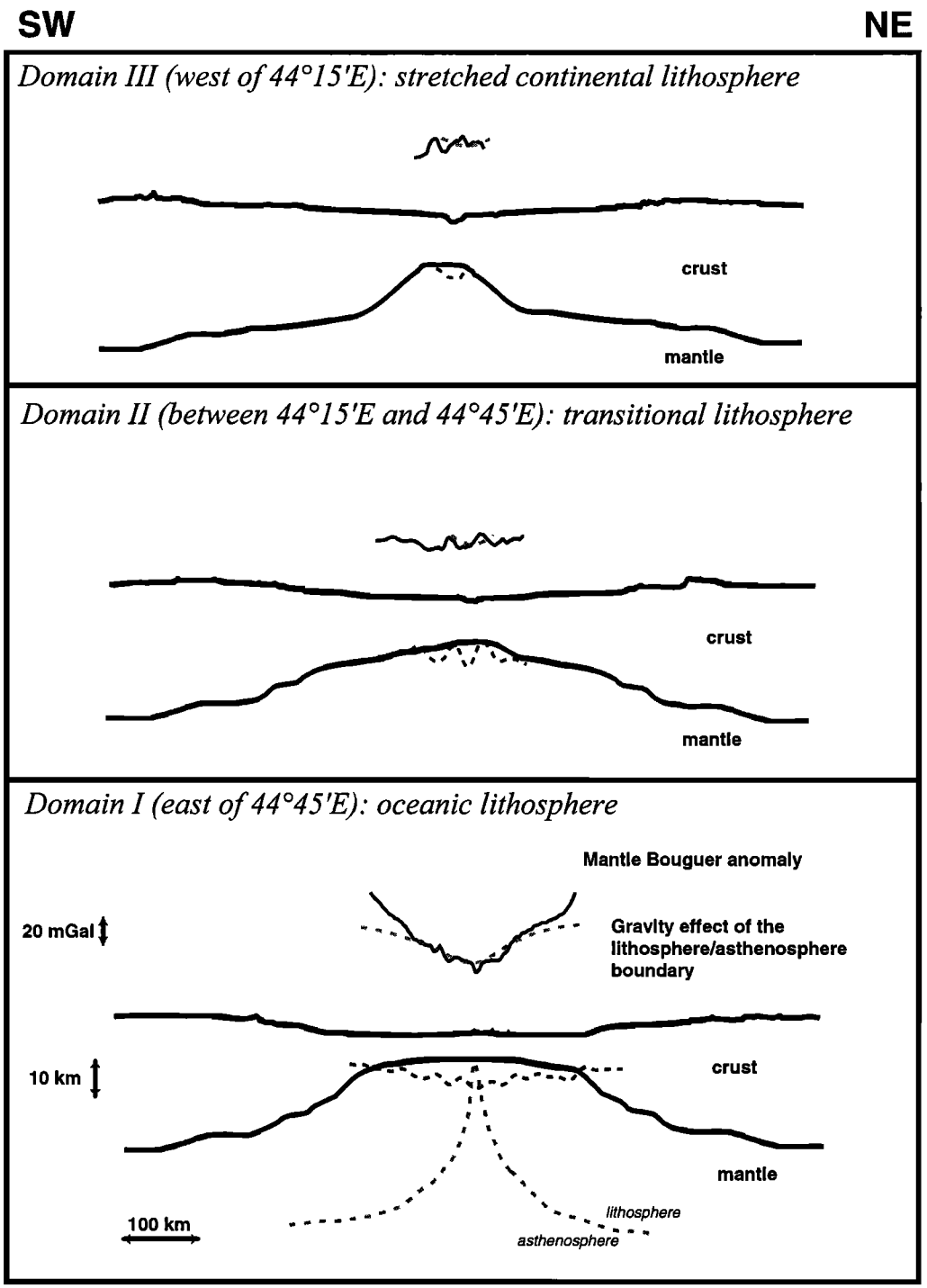

Figure 11. Three different stages of oceanization corresponding to the three areas defined by our results (see limits on Plate 2). For each domain the top solid curve is the Bouguer anomaly, and the dashed one is the estimated thermal gravity effect; the bottom section shows the bathymetry and the Moho (thin dashed line for the Moho obtained from the inversion of gravity data, bold line for a sketch of the realistic Moho when thermal effects are taken into account). Domain I corresponds to an oceanic lithosphere. The lithosphere/asthenosphere boundary is shown with a grey dashed line and corresponds to a thermal subsidence which has occurred for the last 10 Ma. Domain III is more likely associated with stretched continental lithosphere. Domain II seems to be associated with a transitional lithosphere.

seafloor spreading is at its very beginning, and the true oceanic crust could be only present beneath the axial valley. The flanks of the axial valley seem to be underlain by a crustal thinning which may correspond to either a stretched continental crust or a primitive oceanic crust, or a mixture of both. Backscatter data show that axial lava flows west of 44°20'E are not recent [*Dauteuil et al.*, 2001].

The westernmost area (domain III) consists of an essentially stretched continental crust (15-20 km thick), without any seafloor accretion. En echelon basins

perpendicular to the opening direction are not observed at the axis, but a depression underlain by an asymmetric crustal structure (10-13 km thick) is noticed. Active volcanism is restricted to small isolated cones as shown in the backscatter data [*Dauteuil et al.*, 2001].

7.1. Plume-Ridge Interaction

The model of Moho we have assumed and used allows us to account for a regional Bouguer anomaly related to a continent-ocean crustal transition. The analysis of an axial and an off-axis profile (Figure 8) shows that the long-wavelength of the mantle Bouguer anomaly is at first order well explained by this continent-ocean crustal transition. But the axial profile also displays a relative negative gravity anomaly in the oceanic area east of 44°45'E, in agreement with a well-established and hotter upper mantle upwelling. This profile thus suggests that our crustal model combined with an asthenospheric upwelling related to the spreading process explains well our data in the eastern area. In addition, the crustal thickness (about 8 km) we obtain in this oceanic domain I is typical of a normal oceanic crust generated outside any hot spot influence [*White et al.*, 1992]. Thus the thermal influence of a plume is not required there.

However, the morphology of the oblique basins evidenced in the western Aden spreading ridge [*Tamsett and Searle*, 1988; *Dauteuil et al.*, 2001] looks like the morphology of the Reykjanes Ridge south of Iceland [Searle et al., 1998] and of the Mohns Ridge north of Iceland [*Dauteuil and Brun*, 1993]. The oceanic crust is thicker at such spreading ridges located in the vicinity of a hot spot (10-12 km) [*Smallwood and White,* 1998]. The shallowing of the asthenosphere when approaching the hot spot implies a shallowing of the brittle/ductile transition which causes a narrower deformation band. In such a case, a ridge-transform configuration is no more allowed and this yields preferentially a series of en echelon extensional features [*Dauteuil and Brun*, 1993]. In the western Gulf of Aden, we similarly observe en echelon basins and oblique spreading, and the crust is thicker toward the East Africa hot spot. But the main difference is that the western Aden spreading ridge is characterized by a transition from a a new oceanic crust to a stretched continental crust whereas the Reykjanes Ridge is associated with true oceanic crust everywhere.

7.2. Segmentation Pattern and Ridge Propagation

Our results do not allow us to define a segmentation pattern similar to the one described at slow spreading ridges such as the Mid Atlantic Ridge. The morphological expression of the Aden spreading ridge west of 46°E consists of a succession of en echelon basins whose trend is oblique with respect to the opening direction. However, the interpretation of gravity data allows us to identify three lithospheric domains whose EW length ranges from 50 to 80 km and whose characteristics are quite homogeneous.

The three domains do not display any individual morphological signature and are not offset. We note that the limit between domains I and II corresponds to the previously proposed Shukra El Sheikh discontinuity [*Cochran*, 1981]. The transition between the domains II and III corresponds to a local mantle Bouguer anomaly low (44°10'E, Plate 2). It also coincides with the southern end of a submarine canyon observed in bathymetric data (Figure 2) which may hide a tectonic feature. Along axis, discrete pseudocrustal thickenings (1-2 km) occur and have sizes (10-15 km) similar to the size of the oblique basins (Figure 9). However they seem to be preferentially located between these basins. This is in agreement with extension, hence thinning, associated with the basins. Such thickenings might also indicate the presence of small localized asthenospheric upwellings along the axis. However, it is unlikely that these thickenings are related to a higher magmatism since backscatter data do not evidence any associated volcanic activity. The en echelon basins may be therefore better interpreted as extension cells rather than accretion cells.

A recent analysis of the geometry of the inner graben sizes, based on the bathymetry and backscatter data gathered during the Tadjouraden cruise, allows *Dauteuil et al.* [2001] to infer distinct variations in mechanical behavior along the axis and to distinguish three areas defined by distinct thicknesses of the brittle layer. The limits of these three areas are close to ours and allow the definition of a transitional lithosphere in the middle area, where the brittle layer thickness display important variations and is interpreted as a rheological transition between an oceanic domain (in the east) and a continental one (in the west). Such results are very similar to the ones obtained from our independent gravity study.

From both studies, we propose that our domain I corresponds to a typical oceanic lithosphere, domain III still corresponds to a continental lithosphere, and that domain II is characterized by a transitional lithosphere. The transitional crust defined in domain II can be seen as a stretched continental crust where thick blocks are mixed with thinned crust. This domain II may be already affected by localized asthenospheric upwelling, and magnetic anomalies show that a basaltic layer has already recorded the last 2 Ma reversals. However, the mechanism producing magnetic anomalies when oceanic spreading is not well established remains to be investigated.

The three distinct mechanical areas defined in our study suggest that the propagation of the seafloor spreading was discontinuous and rapid. Each individual domain has rapidly propagated westward and has established within 2-3 Ma. After a 1-2 Ma pause the westward propagation resumed. This model can be compared with that proposed for the Woodlark Basin [*Taylor et al.*, 1999], where seafloor spreading is proposed to develop through spreading center nucleation, then propagation (or possible local stall and jump). Nucleation occurs when rifting has been maximal within extensional basins. Similarly, we observe a rapid propagation within each domain. The aborted rift noticed in the basement, north to the active axis (Figure 3), is consistent with a southward jump of the axis before 2 Ma, toward a rheologically weaker stretched area, and this is close to the model of axial jumps proposed by *Taylor et al.* [1999].

The second-order segmentation observed at slow spreading ridges has not a constant architecture through time, since magmatic feeding and segment morphology are not stable, and this segmentation is not expected to be directly inherited from former continental heterogeneities. However, the corresponding mantle pattern could be conceptually related to the very beginning of seafloor spreading, and possibly to late stage of rifting [*Hayward and Ebinger*, 1996]. The domains we define may correspond to successive emplacements of distinct asthenospheric upwellings, and further develop as distinct accretion cells, to eventually evolve as the ones

observed at slow spreading ridges. This model is close to the model of a rift-induced second-order mantle convection, especially recently proposed in the Woodlark Basin [*Martinez et al.*, 1999], and our results suggest that the discontinuous way the ridge propagates should be partly responsible for the subsequent 3-D pattern of the seafloor spreading processes.

Acknowledgments. We are grateful to the Captain, officers and crew of the R/V *L'Atalante* during the Tadjouraden cruise. We thank Michel Diament for fruitful discussions and Olivier Dauteuil for his constructive remarks on a first draft manuscript. Associate Editor C. J. Ebinger and two anonymous referees provided helpful comments to improve the manuscript. All the figures were created using Generic Mapping Tools [*Wessel and Smith*, 1991]. Data processing was funded by a CNRS-INSU grant. Contribution IPGP n° 1730.

References

Acton, G.D., S. Stein, and J.F. Engeln, Block rotation and continental extension in Afar: A comparison to oceanic microplate systems, *Tectonics*, *10*, 501-526, 1991.

Audin, L., Pénétration de la dorsale d'Aden dans la dépression Afar entre 20 et 4 Ma, Thèse de Doctorat, 278 pp., Univ. Paris 7, Paris, France, 1999.

Chapman, M.E., Techniques for interpretation of geoid anomalies, *J. Geophys. Res.*, *84*, 3793-3801, 1979.

Choukroune, P., J. Francheteau, B. Auvray, J.M. Auzende, J.P. Brun, B. Sichler, F. Arthaud, and J.C. Lépine, Tectonics of an incipient oceanic rift, *Mar. Geophys. Res.*, *9*, 147-163, 1988.

Cochran, J.R., The Gulf of Aden: Structure and evolution of a young ocean basin and continental margin, *J. Geophys. Res.*, *86*, 263-287, 1981.

Cochran, J.R., The magnetic quiet zone in the eastern Gulf of Aden: Implications for the early devlopment of the continental margin, *Geophys. J. R. Astron. Soc.*, *68*, 171-201, 1982.

Courtillot, V., A. Galdeano, and J.L. Le Mouël, Propagation of an accreting plate boundary: A discussion of new aeromagnetic data in the Gulf of Tadjoura and southern Afar, *Earth Planet. Sci. Lett.*, *47*, 144-160, 1980.

Courtillot, V., J. Achache, F. Landre, N. Bonhommet, R. Montigny, and G. Féraud, Episodic spreading and rift propagation: New paleomagnetic and geochronologic data from the Afar nascent passive margin, *J. Geophys. Res.*, *89*, 3315-3333, 1984.

Dauteuil, O., and J.-P. Brun, Oblique rifting in a slow-spreading ridge, *Nature*, *361*, 145-148, 1993.

Dauteuil, O., P. Huchon, F. Quéméneur, and T. Souriot, Propagation of an oblique spreading centre: The western Gulf of Aden, *Tectonophysics*, 332, 423-442, 2001.

DeMets, C., R.G. Gordon, D.F. Argus, and S. Stein, Current plate motions, *Geoph. J. Int.*, *101*, 425-478, 1990.

Deplus, C., S. Bonvalot, G. Gabalda, M. Diament, and P. Bachèlery, Bouguer anomaly map of Piton de la Fournaise Volcano constrained by new gravity data, paper presented at the 2nd EVOP Workshop, Santorini, Greece, 1996.

Diament, M., J.-C. Sibuet, and A. Hadaoui, Isostasy of the Northern Bay of Biscay continental margin, *Geophys. J. R. Astron. Soc.*, *86*, 893-907, 1985.

Ebinger, C.J., and N.J. Hayward, Soft plates and hot spots: Views from Afar, *J. Geophys. Res.*, *101*, 21859-21876, 1996.

Egloff, F., R. Rihm, J. Makris, Y.A. Izzeldin, M. Bobsien, K. Meier, P. Junge, T. Noman, and W. Warsi, Contrasting structural styles of the eastern and western margins of the southern Red Sea: The 1988 SONNE experiment, *Tectonophysics*, *198*, 329-353, 1991.

Gaulier, J.M., and P. Huchon, Tectonic evolution of Afar triple junction, *Bull. Soc. Géol. Fr.*, *162*, 451-464, 1991.

Gaulier, J.-M., X. Le Pichon, N. Lyberis, F. Avedik, L. Geli, I. Moretti, A. Deschamps, and S. Hafez, Seismic study of the crust of the northern Red Sea and Gulf of Suez, *Tectonophysics*, *153*, 55-88, 1988.

Gente, P., R.A. Pockalny, C. Durand, C. Deplus, M. Maia, G. Ceuleneer, C. Mével, M. Cannat, and C. Laverne, Characteri-stics and evolution of the segmentation of the Mid-Atlantic Ridge between 20°N and 24°N during the last 10 million years, *Earth Planet. Sci. Lett.*, *129*, 55-71, 1995.

Hayward, N.J., and C.J. Ebinger, Variations in the along-axis segmentation of the Afar Rift system, *Tectonics*, *15*, 244-257, 1996.

Hébert, H., Etudes géophysiques d'une dorsale naissante (dorsale d'Aden à l'Ouest de 46°E) et d'une dorsale fossile (dorsale de Wharton), Thèse de Doctorat, 372 pp., Univ. Paris 7, Paris, France, 1998.

Huchon, P., et al., Propagation de la frontière de plaques Arabie-Somalie, I, le golfe d'Aden occidental, paper presented at Géol. Soc. France, Géosciences Marines, Brest, 1995.

Inoue, H., A least-squares smooth fitting for irregularly spaced data: Finite-element approach using the cubic B-spline basis, *Geophysics*, *51*, 2051-2060, 1986.

Izzeldin, A.Y., Seismic, gravity and magnetic surveys in the central part of the Red Sea: Their interpretation and implications for the structure and evolution of the Red Sea, *Tectonophysics*, *143*, 269-306, 1987.

Jestin, F., P. Huchon, and J.M. Gaulier, The Somalia plate and the East African Rift System: Present kinematics, *Geophys. J. Int.*, *116*, 637-654, 1994.

Keen, C.E., and S.A. Dehler, Extensional styles and gravity anomalies at rifted continental margins: Some North Atlantic examples, *Tectonics*, *16*, 744-754, 1997.

Khanbari, K., Propagation d'un rift océanique: le Golfe d'Aden, Thèse de Doctorat, 222 pp., Univ. Paris Sud, Paris, France, 2000.

Kuo, B.-Y., and D.W. Forsyth, Gravity anomalies of the ridge-transform system in the South Atlantic between 31° and 34.5°S: Upwelling centers and variations in crustal thickness, *Mar. Geophys. Res.*, *10*, 205-232, 1988.

Laughton, A.S., and C. Tramontini, Recent studies of the crustal structure in the Gulf of Aden, *Tectonophysics*, *8*, 359-375, 1969.

Le Pichon, X., and J.-M. Gaulier, The rotation of Arabia and the Levant fault system, *Tectonophysics*, *153*, 271-294, 1988.

Lépine, J.C., and A. Hirn, Seismotectonics in the Republic of Djibouti, linking the Afar depression and the Gulf of Aden, *Tectonophysics*, *209*, 65-86, 1992.

Lin, J., and J. Phipps Morgan, The spreading rate dependence of 3-D mid-ocean ridge structure, *Geophys. Res. Lett.*, 19, 13-16, 1992.

Makris, J., and A. Ginzburg, The Afar depression: Transition between continental rifting and sea-floor spreading, *Tectonophysics*, *141*, 199-214, 1987.

Manighetti, I., P. Tapponnier, V. Courtillot, S. Gruszow, and P.-Y. Gillot, Propagation of rifting along the Arabia-Somalia plate boundary: The Gulfs of Aden and Tadjoura, *J. Geophys. Res.*, *102*, 2681-2710, 1997.

Manighetti, I., P. Tapponnier, P.Y. Gillot, E. Jacques, V. Courtillot, R. Armijo, J.C. Ruegg, and G. King, Propagation of rifting along the Arabia-Somalia plate boundary: Into Afar, *J. Geophys. Res.*, *103*, 4947-4974, 1998.

Martinez, F., B. Taylor, and A.M. Goodwillie, Contrasting styles of seafloor spreading in the Woodlark Basin: Indications of rift-induced secondary mantle convection, *J. Geophys. Res.*, *104*, 12,909-12,926, 1999.

Montagner, J.-P., and T. Tanimoto, Global anisotropy in the upper mantle inferred from the regionalization of phase velocities, *J. Geophys. Res.*, *95*, 4797-4819, 1990.

Neumann, G.A., and D.W. Forsyth, The paradox of the axial profile: Isostatic compensation along the axis of the Mid-Atlantic Ridge?, *J. Geophys. Res.*, *98*, 17,891-17,910, 1993.

Oldenburg, D.W., The inversion and interpretation of gravity anomalies, *Geophysics*, *39*, 526-536, 1974.

Parker, R.L., The rapid calculation of potential anomalies, *Geophys. J. R. Astron. Soc.*, 31}, 447-455, 1972.

Parsons, B., and J.G. Sclater, An analysis of the variation of ocean floor bathymetry and heat flow with age, *J. Geophys. Res.*, 82, 803-827, 1977.

Phipps Morgan, J., and D.W. Forsyth, Three-dimensional flow and temperature perturbations due to a transform offset: Effects on oceanic crustal and upper mantle structure, *J. Geophys. Res.*, *93*, 2955-2966, 1988.

Rommevaux, C., C. Deplus, P. Patriat, and J.-C. Sempéré, Three-dimensional gravity study of the Mid-Atlantic Ridge: Evolution of the segmentation between 28° and 29°N during the last 10 m.y., *J. Geophys. Res.*, *99*, 3015-3029, 1994.

Schilling, J.-G., Afar mantle plume: Rare earth evidence, *Nature Phys. Sci.*, *242*, 2-5, 1973.

Schouten, H., K.D. Klitgord, and J.A. Whitehead, Segmentation of mid-ocean ridges, *Nature*, *317*, 225-229, 1985.

Searle, R.C., J.A. Keeton, R.B. Owens, R.S. White, R. Mecklenburgh, B. Parsons, and S.M. Lee, The Reykjanes Ridge: Structure and tectonics of a hot-spot-influenced, slow-spreading ridge, from multibeam bathymetry, gravity and magnetic investigations, *Earth Planet. Sci. Lett.*, *160*, 463-478, 1998.

Shaw, W.J., and J. Lin, Models of ocean ridge lithospheric deformation: Dependence on crustal thickness, spreading rate, and segmentation, *J. Geophys. Res.*, *101*, 17,977-17,993, 1996.

Sichler, B., La bielette danakile: Un modèle pour l'évolution géodynamique de l'Afar, *Bull. Soc. Géol. Fr.*, *22*, 925-933, 1980.

Sloan, H., and P. Patriat, Kinematics of the North American-African plate boundary between 28° and 29°N during the last 10 Ma: Evolution of the axial geometry and spreading rate and direction, *Earth Planet. Sci. Lett.*, *113*, 323-341, 1992.

Smallwood, J.R., and R.S. White, Crustal accretion at the Reykjanes Ridge, 61°-62°N, *J. Geophys. Res.*, *103*, 5185-5201, 1998.

Smith, W.H.F., and D.T. Sandwell, Global sea floor topography from satellite altimetry and ship depth soundings, *Science*, *277*, 1956-1962, 1997.

Souriot, T., and J.-P. Brun, Faulting and block rotation in the Afar triangle, East Africa: The Danakil "crank-arm" model, *Geology*, *20*, 911-914, 1992.

Stein, C.A., and S. Stein, A model for the global variation in oceanic depth and heat flow with lithospheric age, *Nature*, *359*, 123-129, 1992.

Tamsett, D., An application of the response function technique to profiles of bathymetry and gravity in the Gulf of Aden, *Geophys. J. R. Astron. Soc.*, *78*, 349-369, 1984.

Tamsett, D., and R.C. Searle, Structure and development of the midocean ridge plate boundary in the Gulf of Aden: Evidence from GLORIA side scan sonar, *J. Geophys. Res.*, *93*, 3157-3178, 1988.

Tapponnier, P., R. Armijo, I. Manighetti, and V. Courtillot, Bookshelf faulting and horizontal block rotations between overlapping rifts in southern Afar, *Geophys. Res. Lett.*, *17*, 1-4, 1990.

Taylor, B., A.M. Goodlife, and F. Martinez, How continents break up: Insights from Papua New Guinea, *J. Geophys. Res.*, *104*, 7497-7512, 1999.

Tolstoy, M., A.J. Harding, and J.A. Orcutt, Crustal thickness on the Mid-Atlantic Ridge: Bull's-eye gravity anomalies and focused accretion, *Science*, *262*, 726-729, 1993.

Tucholke, B.E., J. Lin, M.C. Kleinrock, M.A. Tivey, T.B. Reed, J. Goff, and G.E. Jaroslow, Segmentation and crustal structure of the western Mid-Atlantic Ridge flank, 25°25'-27°10'N and 0-29 m.y., *J. Geophys. Res.*, *102*, 10,203-10,223, 1997.

Vidal, P., C. Deniel, P.J. Vellutini, P. Piguet, C. Coulon, J. Vincent, and J. Audin, Changes of mantle sources in the course of a rift evolution: The Afar case, *Geophys. Res. Lett.*, *18*, 1913-1916, 1991.

Wessel, P., and W.H.F. Smith, Free software helps map and display data, *Eos Trans. AGU*, *72*, 441, 445-446, 1991.

White, R.S., D. McKenzie, and R.K. O'Nions, Oceanic crustal thickness from seismic measurements and rare earth element inversions, *J. Geophys. Res.*, *97*, 19,683-19,715, 1992.

L. Audin, Laboratoire de Tectonique et Mécanique de la Lithosphère, UMR 7578 Centre National de la Recherche Scinetifique (CNRS), Institut de Physique du Globe, 4, place Jussieu, 75252 Paris Cedex 05, France.

C. Deplus and H. Hébert, Laboratoire de Gravimétrie et Géodynamique, UMR 7577 CNRS, Institut de Physique du Globe, 4 place Jussieu, 75252 Paris Cedex 05, France. (hebert@ipgp.jussieu.fr).

P. Huchon, Géosciences Azur, UMR 6526 CNRS, Observatoire océanologique de Villefranche-sur-Mer, BP 28, 06234 Villefranche-sur-Mer, France.

K. Khanbari, Faculty of Sciences, Department of Geology, University of Sana'a, Sana'a, Republic of Yemen.

(Received December 15, 1999; revised October 12, 2000;
accepted October 19, 2000.)